Evolution of the Onset of Coherence in a Diode Laser

PC4199 Honours Project in Physics

Alvin Leow

A0155921E

Advisor: Christian Kurtsiefer

A thesis presented for the degree of

Bachelor of Science (Hons)

Centre for Quantum Technologies

Department of Physics, Faculty of Science

National University of Singapore

Acknowledgements

First, I would like to thank Prof Christian for giving me the opportunity to work on this project, and for showing so much patience and encouragement throughout the duration.

To Peng Kian, who guided me throughout the entire project - thank you. You have taught me much about the subject, but even more about the thought processes behind conducting a scientific experiment. From tirelessly asking questions to prompt me to think more about the rationale behind my actions, to putting up with my ignorance and slip ups along the way, I am truly grateful for everything you have taught me.

To Xi Jie, thank you for being the great office mate and knowledgable senior that I can bug whenever I have questions, and helping to guide me along in this project. I really enjoyed the late night lab sessions, dinners and random conversations with you and Peng Kian.

To everyone else in the Quantum Optics group, thank you for all the help rendered along the way in one way or another, and for being a great group of people to be around.

Before I had embarked on this project, I was clueless about how scientific research is conducted. It has indeed been an eye-opening experience as a first foray into research. Although this has not been an easy journey, it is definitely one of the most important milestone of my undergraduate life. Perhaps, this is a reminder of why I love Physics so much in the first place.

"I have loved the stars too fondly to be fearful of the night."

Abstract

Although the second-order coherence of a light source is often raised as a potential candidate for a defining trait of a laser [Blood, 2013], it has yet to be experimentally measured for semiconductor laser diodes. Previous measurements of second-order coherence, usually realised by measurement of intensity correlation, have focused largely on microcavity lasers [Ulrich et al., 2007], [Wiersig et al., 2009], [Wang et al., 2017]. In this report, we attempt to utilise a narrowband spectral filtering method [Liu et al., 2014], [Tan et al., 2014] to increase the coherence time of laser diode in LED mode, and henceforth measure its intensity correlation.

By examining the intensity correlation of light from a laser diode over an input current range of 30 mA to 36 mA, we observe four possible regimes of a laser diode as it transitions from an LED to laser. During this transition phase, as input current increases, we first observe the narrowing of laser diode linewidth as coherence time τ_c increases from 0.256 ns to 0.722 ns, and an increase in the second-order correlation while the $g^{(2)}(\tau{=}0)$ changes from 1.14 at I = 30.00 mA to 1.92 at I = 31.51 mA. Subsequently, while τ_c of the laser diode beam continues to increase with increasing input current, the intensity correlation $g^{(2)}(\tau{=}0)$ begins to drop, and the laser diode finally transitions into a coherent laser source.

Contents

List of Figures

Chapter 1

Introduction

1.1 The Laser

The first Maser, or Microwave Amplification by Stimulated Emission of Radiation, was first produced in the 1950s by C.H. Townes [Gordon et al., 1955], based on the theoretical work of Einstein in 1917 [Einstein, 1917]. Schawlow and Townes extended this principles of maser techniques to the infrared and optical domain [Schawlow and Townes, 1958], which would eventually be termed Laser (Light Amplification by Stimulated Emission of Radiation). Using this, Maiman demonstrated the first laser that we know of today [Maiman, 1960].

The laser differs from other light sources in its coherence. We distinguish here between two types of coherence, spatial and temporal, and focus the subsequent discussion on the temporal coherence of light.

In a rump session of the International Semiconductor Laser Conference in 2012, a question was addressed, 'What is a laser?' [Blood, 2013], with particular reference to diode lasers. While this question was posed to invoke thought in view of new devices such as single-photon source and nanolasers, it nevertheless brings about some food for thought: Does the coherence of a light source define lasing action?

In this report, we attempt to measure the second-order coherence of a semi-conductor laser diode as it transitions from LED to laser light. While this does not answer the question 'What is a laser?' directly, it provides an experimental consideration to the question by measuring a quantity which some considers a defining physical quantity of a laser.

1.2 Temporal Coherence

The temporal coherence of a light source is described by its coherence time τ_c, which also determines the spectral width of the beam.

$$\tau_c \approx \frac{1}{\Delta\nu} \tag{1.1}$$

Thus, an ideal monochromatic source has infinite τ_c, and an effective $\Delta\nu$ of 0. However, the ideal monochromatic source does not exist as we know it. The theoretical minimum linewidth for a laser was derived in 1955 [Gordon et al., 1955], as given by the Schawlow-Townes equation

$$\Delta\nu_{laser} = \frac{4\pi h\nu(\Delta\nu_c)^2}{P_{out}} \tag{1.2}$$

For a given light source, resonator bandwidth $(\Delta\nu_c)^2$ remains constant, while central frequency ν remains approximately constant. We thus obtain

$$\Delta\nu_{laser} \propto \frac{1}{P_{out}} \tag{1.3}$$

Most light sources are partially coherent, and we define their coherence by the first-order correlation function, $g^{(1)}$[Fox, 2006]

$$g^{(1)}(\tau) = \frac{< \epsilon^*(t)\epsilon(t+\tau) >}{< |\epsilon(t)|^2 >} \tag{1.4}$$

For a quasi-monochromatic light source of

$$\epsilon(t) = \epsilon_0 e^{-i\omega_0 t} e^{i\phi(t)} \tag{1.5}$$

where ω_0 is its centre frequency, we measure its correlation function using a Michelson interferometry experiment

$$|g^{(1)}(\tau)| = visibility = \frac{I_{max} - I_{min}}{I_{max} + I_{min}} \tag{1.6}$$

1.3 Intensity Interferometry

The intensity interferometer was developed by R. Hanbury Brown and R. Q. Twiss as a way to carry out stellar observations beyond the diffraction limit of a collection mirror [Hanbury Brown and Twiss, 1956].

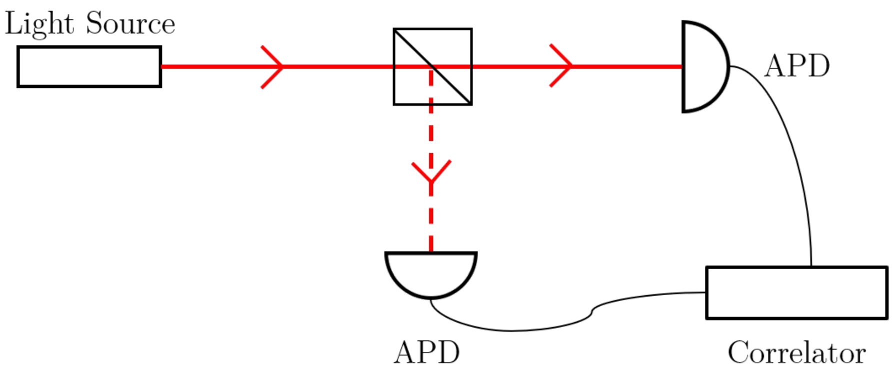

Figure 1.1: Basic second-order correlation measurement setup

Figure 1.1 shows a simplified schematic of an intensity interferometer setup. The basic idea behind the measurement is to split a light beam (Hanbury Brown and Twiss used the 435.8nm emission line from a mercury (Hg) discharge lamp) via a beam splitter, and detect the two beams with avalanche photodetectors (APDs). The electronic signal by one of the APDs (e.g. the reflected arm) will be passsed through a time delay generator with delay timing τ. We define the second-order coherence by the second-order correlation function of the light [Fox, 2006]

$$\begin{aligned} g^{(2)}(\tau) &= \frac{< I(t)I(t+\tau) >}{< I(t) >< I(t+\tau) >} \\ &= \frac{< n_1(t)n_2(t+\tau) >}{< n_1(t) >< n_2(t+\tau) >} \end{aligned} \tag{1.7}$$

where n_1 is the photon count on the APD without timing delay, and n_2 is the photon count on the APD with timing delay τ. This means that $g^{(2)}(\tau)$ is dependent on the simultaneous probability of detecting photons at time t at APD 1 and time $t+\tau$ at APD 2. We generalise this expression to the probabilities of two-photon coincidence events,

$$g^{(2)}(\tau) = \frac{P_{1,2}}{P_1 P_2} \tag{1.8}$$

Thus, in our experimental scheme, the g(2) function is measured by the histogram of two-photon coincidence events, with the second-order correlation ($g^{(2)}(\tau = 0)$) value calculated by the probability of observing a photon at time t at APD 1 and time $t+\tau$ at APD 2, normalised to the probability of an uncorrelated detection [Mandel and Wolf, 1995]. It it also related to the first-order correlation function via

$$g^{(2)}(\tau) = 1 + |g^{(1)}(\tau)|^2 \tag{1.9}$$

1.4 Photon Statistics of Light Source

Classically, we write the electric field of a perfectly coherent light wave as

$$\epsilon(x,t) = \epsilon_0 \sin(kx - \omega t + \phi) \tag{1.10}$$

with a constant angular velocity ω and phase ϕ. A light source which reasonably approximates such a field is a single-mode laser operating above threshold [Fox, 2006].

By considering a light beam with a constant power P, we obtain the photon statistics for a coherent light as

$$P(n) = \frac{\bar{n}^n}{n!} e^{-\bar{n}}, n \in \mathbb{Z}^+ \tag{1.11}$$

which describes a Poisson distribution. In a Poisson distribution, the standard deviation Δn of a mean value n is given by

$$\Delta n = \sqrt{\bar{n}} \tag{1.12}$$

However, if we allow the power P to fluctuate, we can observe the correspondingly larger fluctuations in photon numbers, where

$$\Delta n > \sqrt{\bar{n}} \tag{1.13}$$

and exhibits super-Poissonian statistics. Light sources with sub-Poissonian statistics also exist, but they are beyond the scope of this report and we will not discuss them further. In general, light sources can be classified into three groups[1]:

Photon Statistics	Standard Deviation	$g^{(2)}(\tau=0)$	Photon Stream
Super-Poissonian	$\Delta n > \sqrt{\bar{n}}$	>1	Bunched
Poissonian	$\Delta n = \sqrt{\bar{n}}$	1	Random
Sub-Poissonian	$\Delta n < \sqrt{\bar{n}}$	<1	Antibunched

Table 1.1: Classification of light by photon statistics

An example of a light source which obeys Poissonian statistics is coherent light such as a laser, while an example of a light source which obeys super-Poissonian statistics is thermal light, or blackbody radiation.

[1]We note that while non-classical light show both photon antibunching and sub-Poissonian photon statistics, sub-Poissonian photon statistics need not be associated with photon antibunching [Zou and Mandel, 1990]. However, as we do not investigate these two phenomena in this report, we will not pursue the difference further.

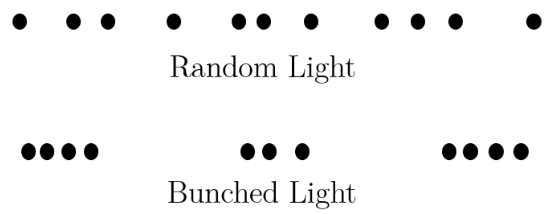

Figure 1.2: Photon stream for bunched and random (coherent) light

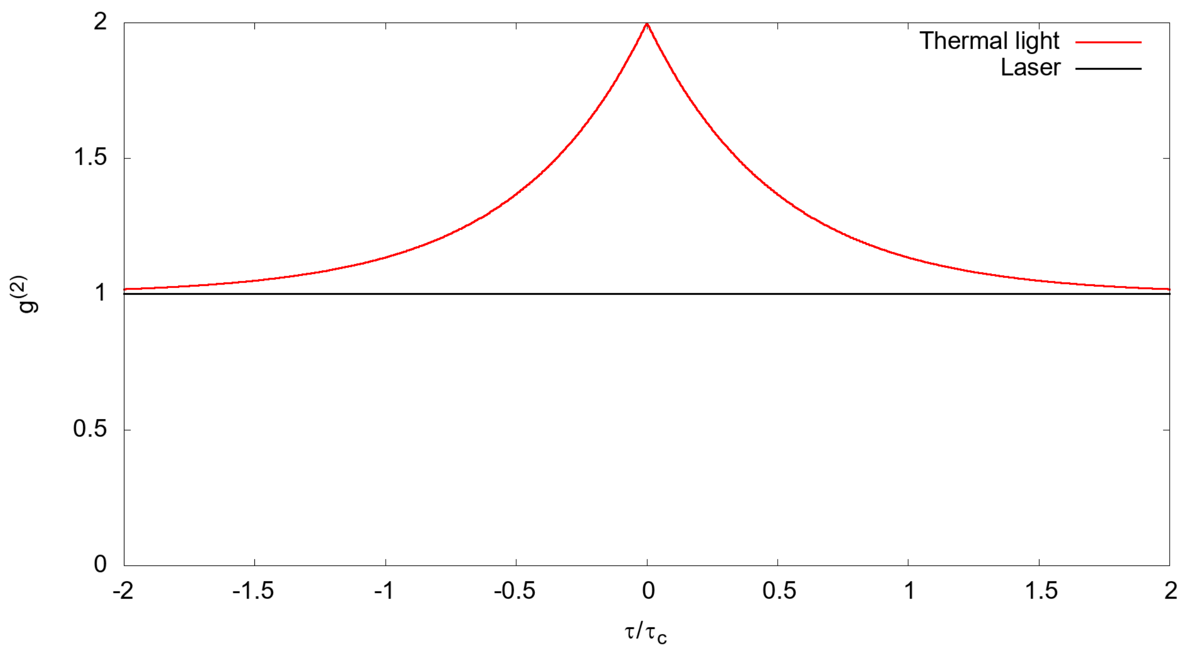

Figure 1.3: Theoretical second order correlation ($g^{(2)}(\tau)$) plot for thermal and laser light

1.5 Experiments on the coherence of lasers near threshold

While the $g^{(2)}(\tau = 0)$ value for coherent light sources has been theorised by Glauber since 1963 [Glauber, 1963], the value of $g^{(2)}(\tau = 0)$ for a semiconductor laser diode has yet to be definitively experimentally verified.

Previous measurements of second-order correlations have focused on the photon statistics of microcavity lasers [Ulrich et al., 2007], [Wiersig et al., 2009], [Wang et al., 2017]. Theoretical calculations on the second-order correlations of nanolasers [Chow et al., 2014] have also been examined, but direct experimental measurement on the $g^{(2)}$ of semiconductor diode lasers remains lacking.

This is in part due to the short coherence time of laser diodes in the LED regime, typically in the order of 10^{-13} s, much shorter than the timing resolution of the best commercial photodetectors, which are in the order of 10^{-11}s.

For a Lorentzian linewidth, the second-order correlation is given by [Fox, 2006]:

$$g^{(2)}(\tau) = 1 + e^{\frac{-2|\tau|}{\tau_c}} \tag{1.14}$$

The $g^{(2)}(\tau=0)$ is only significantly >1 in the LED regime when the coherence time of the light source τ_c is of the order of the timing resolution of the detector. For this report, to resolve a $g^{(2)}(\tau=0)$ of >1 within a reasonable integration time (in the order of 10^2s), we need to be able to filter a bandwidth of light that has coherence time an order of magnitude greater than the timing resolution of the detectors used.

Recent experiments [Tan et al., 2014] [Tan et al., 2016] have been able to employ narrowband spectral filtering techniques via the use of etalons to obtain $g^{(2)}(\tau=0)$ values of blackbody radiators significantly greater than 1, with $g^{(2)}(\tau=0)$ values reaching as high as 1.94 [Deng et al., 2019] for the sun. In this project, we aim to apply a similar spectral filtering technique to filter a narrowband of light in the LED regime of a laser diode to quantify the onset of temporal coherence in a semiconductor laser diode.

Chapter 2

Lasing Regime of a Semiconductor Laser Diode

2.1 Power-Current Curve

Practically, the threshold current of a laser diode - where it transitions from LED to lasing - is usually identified via a kink in the output power (P) to input current (I), the P-I curve [Ning, 2013], [Saleh and Teich, 2019]. While this does not guarantee that a laser diode has transitioned from LED to lasing, it is nonetheless a reasonable indicator to determine the approximate LED and lasing regimes of a semiconductor diode. Thus, in this segment of the experiment, we vary the input current to the laser diode and measure its output power to determine this approximate regime where the transition happens.

The laser diode used is a semiconductor laser diode (Thorlabs L515A1), with a design centre wavelength of 515 nm and 10 mW maximum output power. It is rated for a maximum operating current of 120 mA, and has a threshold current of 30 mA at 25°C.

To obtain an estimate of the lasing threshold, we vary the input current from 1 mA to 60 mA and measure its output power. The temperature of the laser diode peltier was set to a temperature of 20°C. Using a digital powermeter, we align the detection area of the powermeter to the output beam, and note the power reading registered. We vary the input current by a step size of 1 mA, and recorded its output power. This process was then automated by a bash script.

From figure 2.1, we note that there is a sharp increase in output power as the input current increases from 33 mA to 34 mA. We take finer power readings in the neighbourhood of this sharp increase, varying the input current in smaller steps sizes of 0.01 mA from 30 mA to 36 mA, and obtain the the P-I curve in figure 2.2.

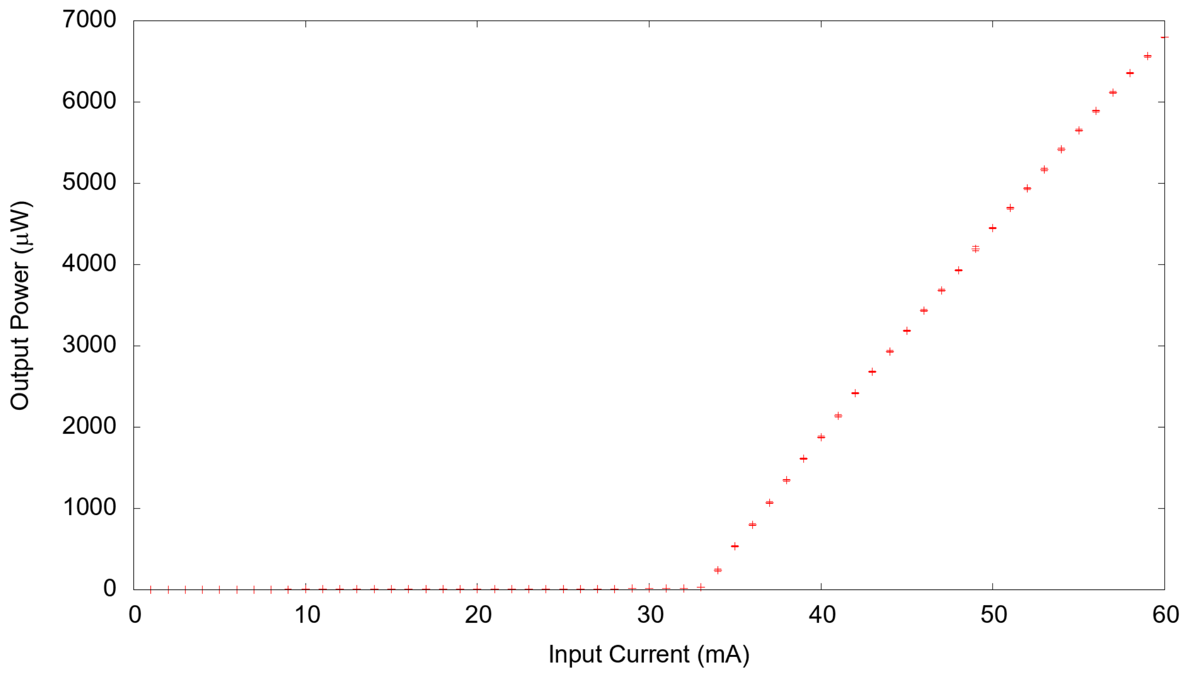

Figure 2.1: P-I curve of laser diode, range = 1 mA to 60 mA, stepsize = 1 mA, temperature = 20°C

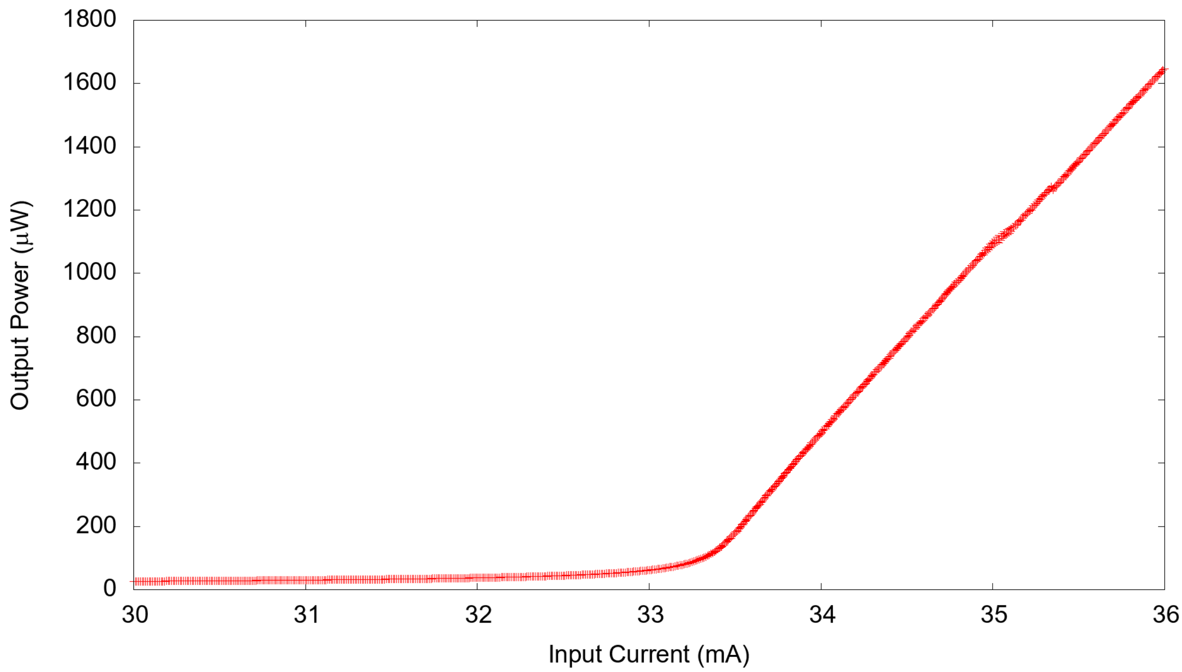

Figure 2.2: P-I curve of laser diode, range = 30 mA to 36 mA, stepsize = 0.01 mA, temperature = 20°C

From Figure 2.2, we see two regimes of the P-I curve, each varying linearly with the input current, and a kink between the two regimes. Taking the differential of the P-I curve, we obtain the plot in figure 2.3.

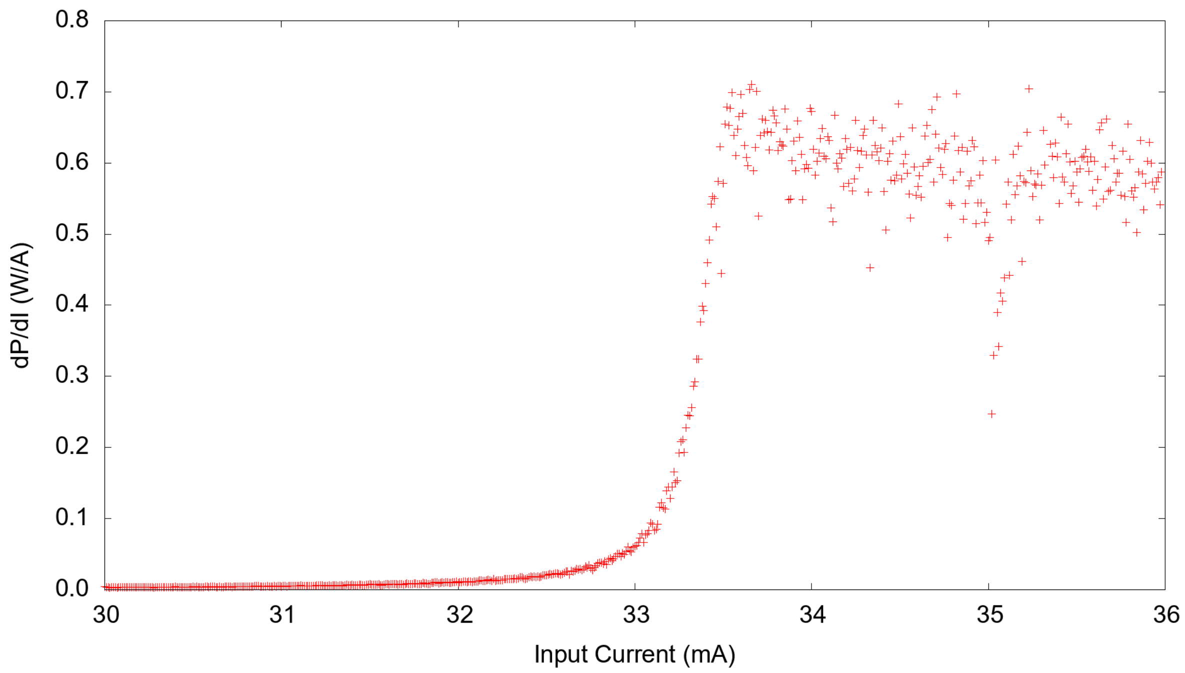

Figure 2.3: $\frac{dP}{dI}$-current curve, range = 30 mA to 36 mA, stepsize = 0.01 mA, temperature = 20°C

From figures 2.2 and 2.3, we can identify three regimes in the graph. When $\mathrm{I} < 32\,\mathrm{mA}$, $\frac{dP}{dI}$ is approximately constant as input current increases, and we term it the 'LED regime'. When $\mathrm{I} > 34\mathrm{mA}$, $\frac{dP}{dI}$ also remains approximately constant (at a higher value) as input current increase, and we term it the 'lasing regime'.

At $32\,\mathrm{mA} < \mathrm{I} < 34\,\mathrm{mA}$, $\frac{dP}{dI}$ increases significantly with input current, suggesting that there is some form of transition between the LED regime and the lasing regime. For now, we term this the 'transition regime'.

We then compare the P-I curve of the laser diode to a green Light-Emitting Diode (LED). As seen in figure 2.4, within the current rating of an LED, its output power does not exhibit a sharp increase at a specific input current value, unlike a laser diode. This suggests that the light emitted by a laser diode does indeed fall into two types (LED and lasing), unlike an LED.

Further, from figures 2.2 and 2.3, we see that the transition between the two mechanisms happens over an input current range of a few milliamperes, as opposed to a step function.

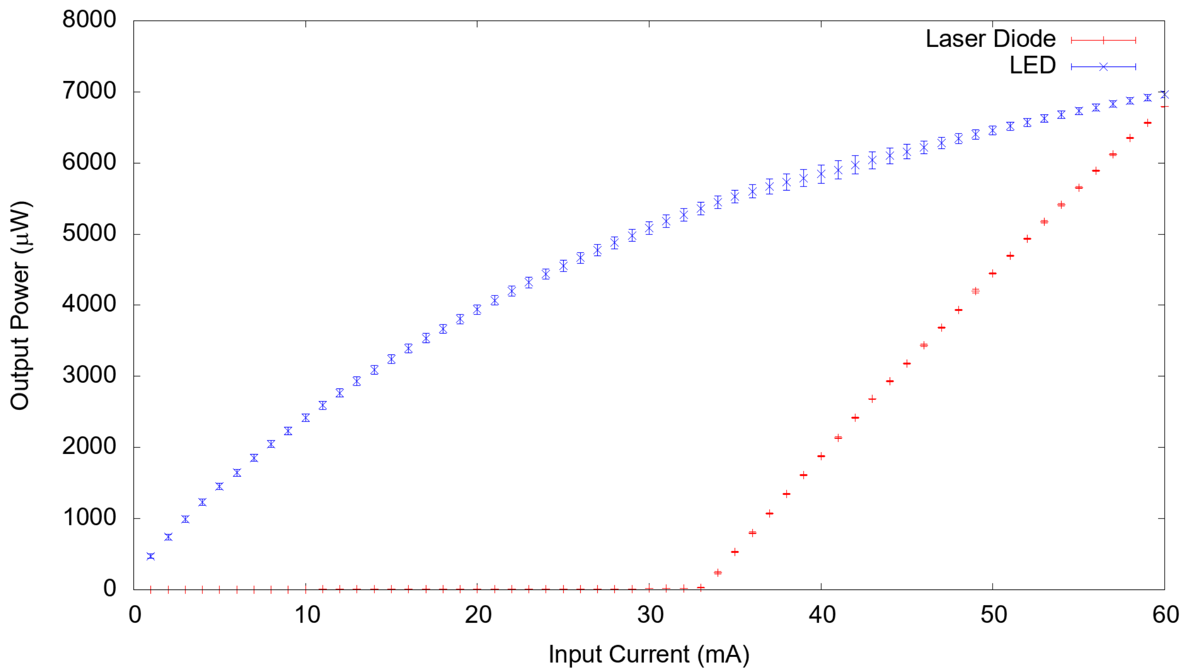

Figure 2.4: Comparison of P-I curves between a laser diode and LED

2.2 Spectrum

Other than the P-I curve, another indicator of the transition regime of a laser diode is the change in the linewidth of the emitted light. As mentioned in chapter 1, as a laser diode transitions from LED to lasing, the linewidth of the light it emits is expected to become narrower. In this section, we investigate the response of the laser diode linewidth while varying the input current.

Light is coupled from the laser diode (Thorlabs L515A1) into a multi-mode fibre via an aspheric lens (Thorlabs C220), which is then sent to a spectrometer for analysis. The spectrometer we use is an Ocean Optics 2000+ unit, rated for operation from 399 nm to 731 nm. The plot of the variation of intensity against the wavelength gives us the spectral information of the laser diode. We analyse and compare the spectrum of the laser diode in the LED regime ($I = 30\,\mathrm{mA}$) and the lasing regime ($I = 36\,\mathrm{mA}$) and obtain figure 2.5

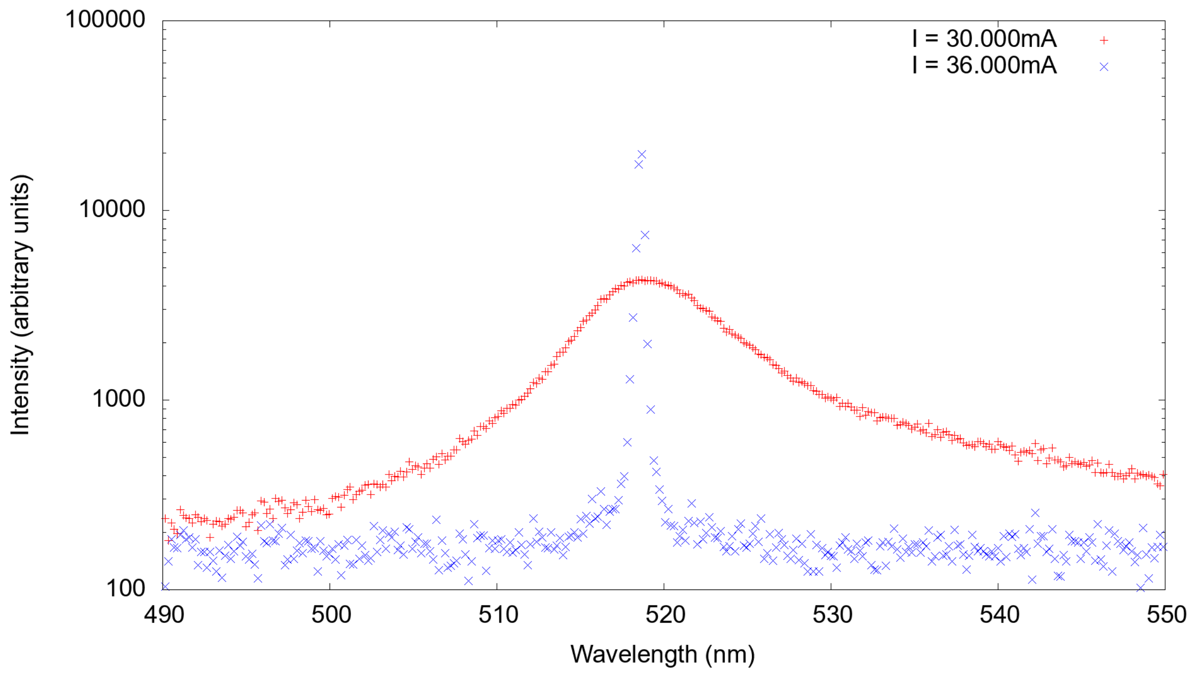

Figure 2.5: Spectrum of laser diode at I = 30.00 mA ('LED regime') and I = 36.00 mA ('lasing regime'). The intensity of the spectrum is plotted using a logarithmic scale.

We see that the linewidth of laser diode decreases significantly as input current increases from 30 mA to 36 mA. Using a Gaussian fit

$$Intensity = a\frac{1}{b\sqrt{2\pi}}e^{-\frac{1}{2}(\frac{x-c}{b})^2} + d \qquad (2.1)$$

we obtain the standard deviation of the distribution as parameter b, which is related to the full-width at half-maximum (FWHM) of the curve by

$$FWHM = 2\sqrt{2\ln 2}\; b \approx 2.355\; b \qquad (2.2)$$

We measure the spectrum of the laser diode while varying input current from 1 mA to 60 mA in stepsize of 1 mA. Next, we fit the spectrum to equation 2.1, and use equation 2.2 to determine its FWHM. Plotting this against input current, we obtain figure 2.6

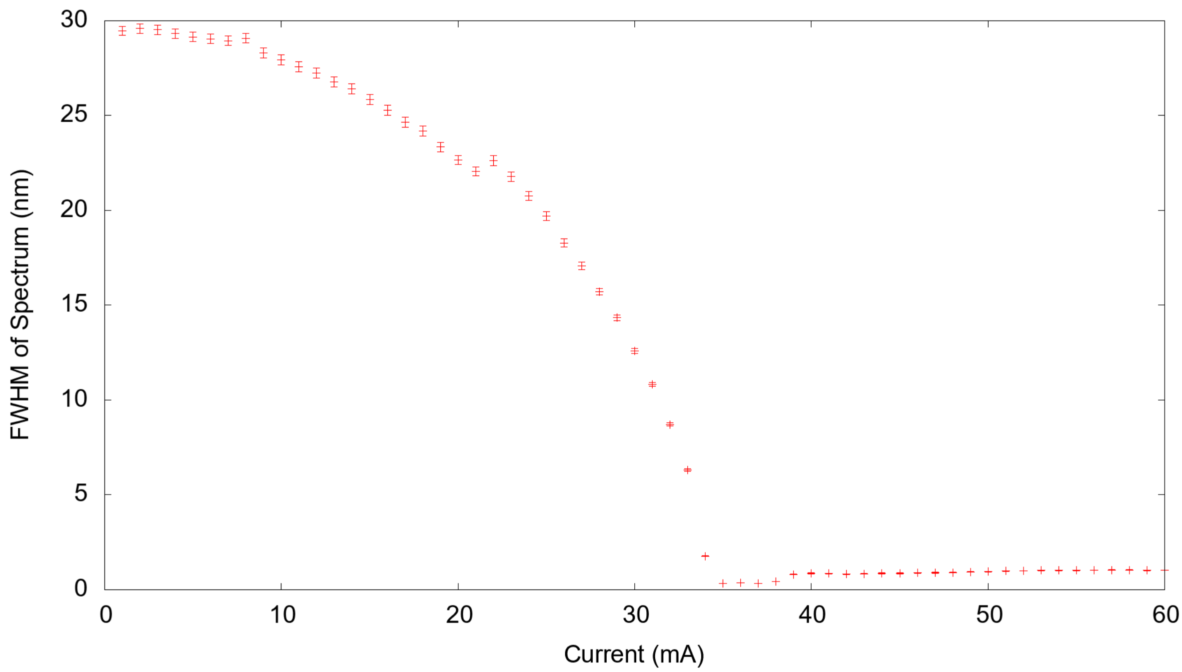

Figure 2.6: Spectral FWHM of laser diode against current, temperature = 20°C, range = 1 mA to 60 mA, stepsize = 1 mA

We measure the spectral FWHM of the laser diode from 30 mA to 60 mA, in smaller stepsizes of 0.1 mA, and obtain figure 2.7.

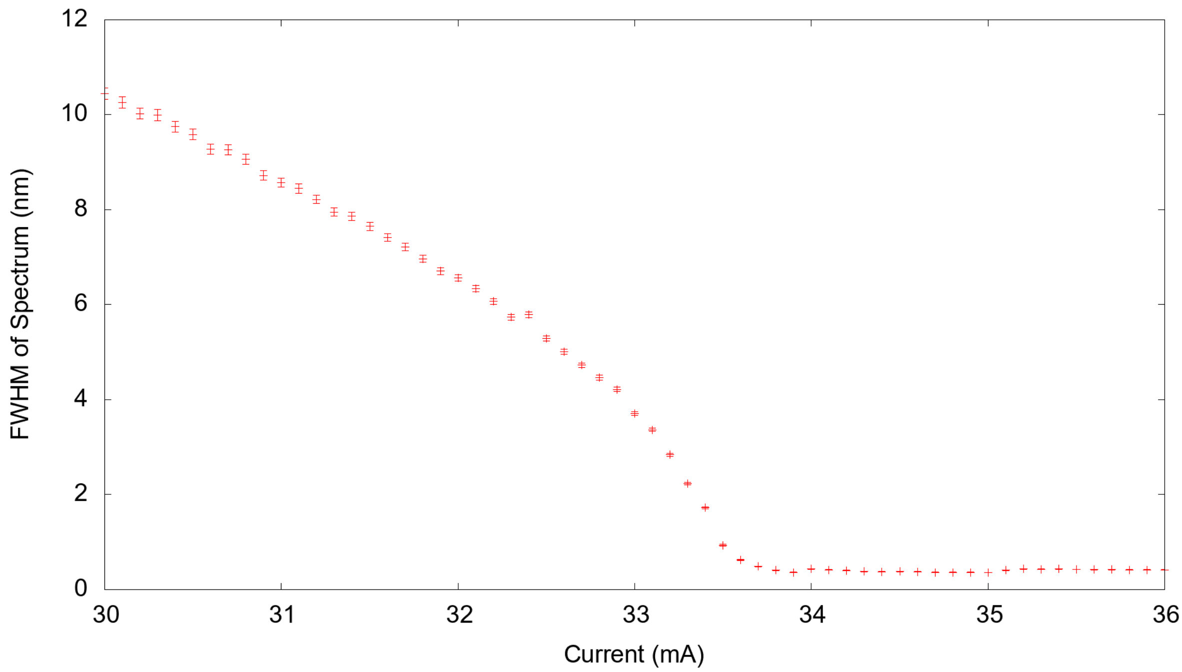

Figure 2.7: Spectral FWHM of laser diode against current, temperature = 20°C, range = 30 mA to 36 mA, stepsize = 0.1 mA

From figures 2.6 and 2.7, we see that the spectral FWHM of the laser diode decreases most rapidly near around $32\,\text{mA} < I < 34\,\text{mA}$, which agrees with the previously identified transition regime in section 2.1.

We also compare the spectral FWHM plot of the laser diode with a green LED in figure 2.8, and find that unlike a laser diode, the spectral FWHM of an LED remains relatively constant as input current varies. This is evidence that as input current to a laser diode increases, its emission linewidth decreases, which indicates an increase in temporal coherence.

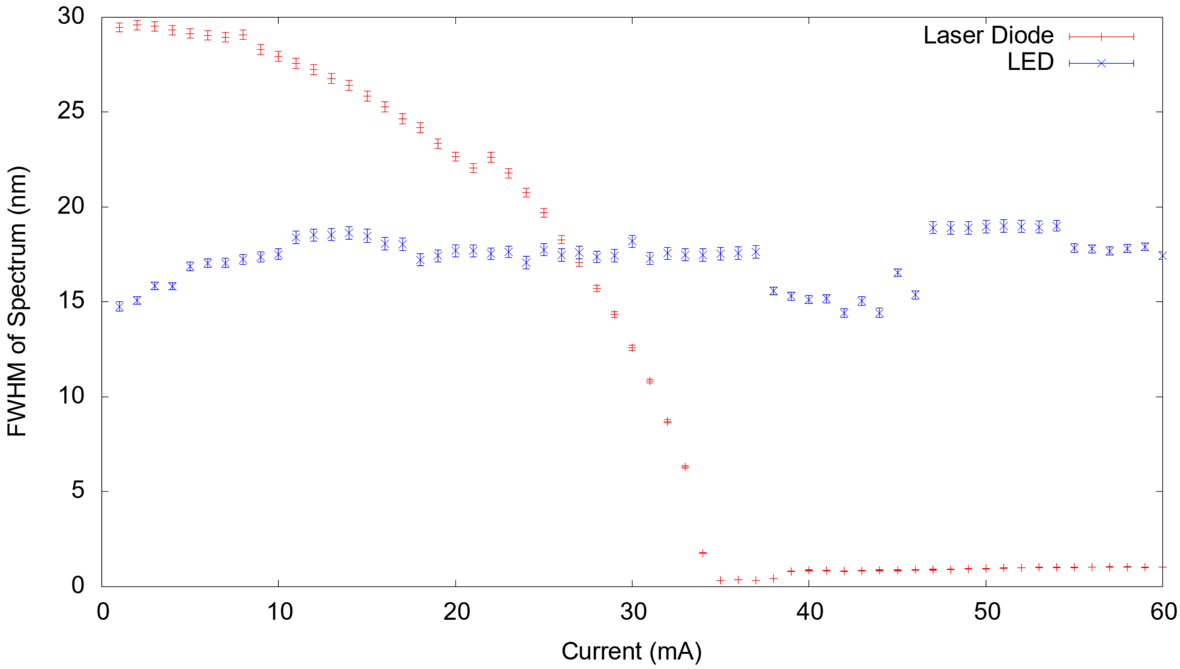

Figure 2.8: Evolution of spectral FWHM with input current for laser diode and LED

Chapter 3

Temporal Intensity Interferometry

3.1 Temporal Intensity Interferometry Setup

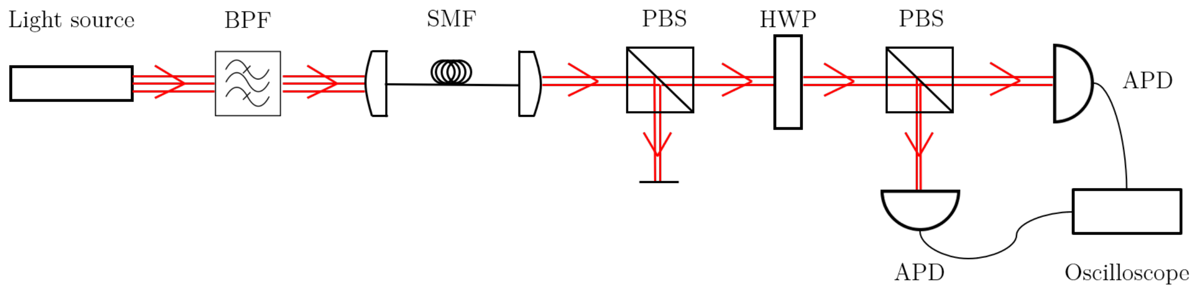

Figure 3.1: Experimental Setup for a Two-Photon Coincidence Measurement

Figure 3.1 is the schematic of the experimental setup to measure the two-photon coincidence of a light source. We couple light from a Mercury (Hg) discharge lamp, a quasi-thermal light source, through a bandpass filter centred at 546 nm, with a nominal Full-Width Half-Maximum of (FWHM) 3 nm into a multimode fibre (MMF, Thorlabs M31L02). We then couple the light into a single mode fibre (SMF, Thorlabs P5-460A) with a numerical aperture (NA) of 0.12. This allows us to select a single spatial mode and enforce the spatial coherence of the beam. This is done to maximise the temporal photon bunching ($g^{(2)}(\tau{=}0)$) signal, which is related to the number of spatial modes M by [Glauber, 1963]:

$$g^{(2)}(\tau = 0) \propto 1 + \frac{1}{M} \tag{3.1}$$

Light exiting from the SMF is then collimated by an aspheric lens (Thorlabs C220) and passed through a Calcite Glan-Taylor polariser (Thorlabs GT10) with an transmission extinction ratio greater than 100,000:1, with a wavelength range from 350nm to 2300nm. This selects a highly linearly polarised light through the transmission arm of the Glan-Taylor polariser. Since the reflected escape beam is not fully polarised, we will not be using the reflected beam for further analysis.

Using a half-wave plate (HWP), we rotate the polarisation of the polarised light by approximately 45° before passing it through a polarising beam splitter (Thorlabs PBS251). The light beam is split into an approximately 50:50 ratio, which will maximise the number of co-incidence events detected by the APDs during the g(2) measurement [1]. The configuration of the two PBS also helps to suppress cross-talk coincidence events from the breakdown flash of the APDs [Kurtsiefer et al., 2001], which can introduce false coincidences.

The light from each arm of the PBS is coupled into a multimode fibre (MMF), which in turn is connected to the avalanche photodetectors (APDs).

The APDs used are actively-quenched grade A single photon avalanche diodes from Micro-Photon Devices, with a timing jitter FWHM of 40 ps. This APD was chosen over a passively-quenched detector such as Perkin-Elmer C30902, with a timing jitter FWHM of 1.2 ns (characterised by [Tan et al., 2014]). Since the temporal photon bunching signal is a convolution of the detector response with the coherence time of the light under analysis, an APD with a smaller timing jitter would increase the photon bunching signal, which allows us to reduce the integration time required to obtain a significant signal.

The detectors are connected to a USB timestamp device via the Transistor-Transistor Logic (TTL) protocol to obtain the count rate of the incident photons. This allows us to optimise the alignment and coupling efficiency among the multiple optical elements.

The APDs are also connected to a digital oscilloscope (Lecroy Waverunner 8404M) with 4 GHz bandwidth, 40 Gsamples/sec via Nuclear Instrumentation Module (NIM) output. We then introduce a timing delay by increasing the length of the RG-58 coxial cables used in the triggering reflected arm of the setup. In coaxial cable, the speed of an electronic signal is approximately $\frac{2}{3}$ of the speed of light in vacuum ($\approx 2 \times 10^8$ m/s), which gives us a timing delay of about 5 ns for every 1 m of co-axial cable used.

The optical signals received by the APDs are time-stamped by the digital oscilloscope. When a photo-event is detected by the APD, its NIM output generates a pulse signal of approximately -700 mV deep and 20 ns wide, as seen in figure 3.2. Using the time@level function of the oscilloscope, such a signal from the reflected arm serves as a trigger signal. The oscilloscope then identifies a qualifier signal from the transmitted arm within the 20 ns hold-off time chosen, shown in figure 3.3.

[1] Refer to Appendix A

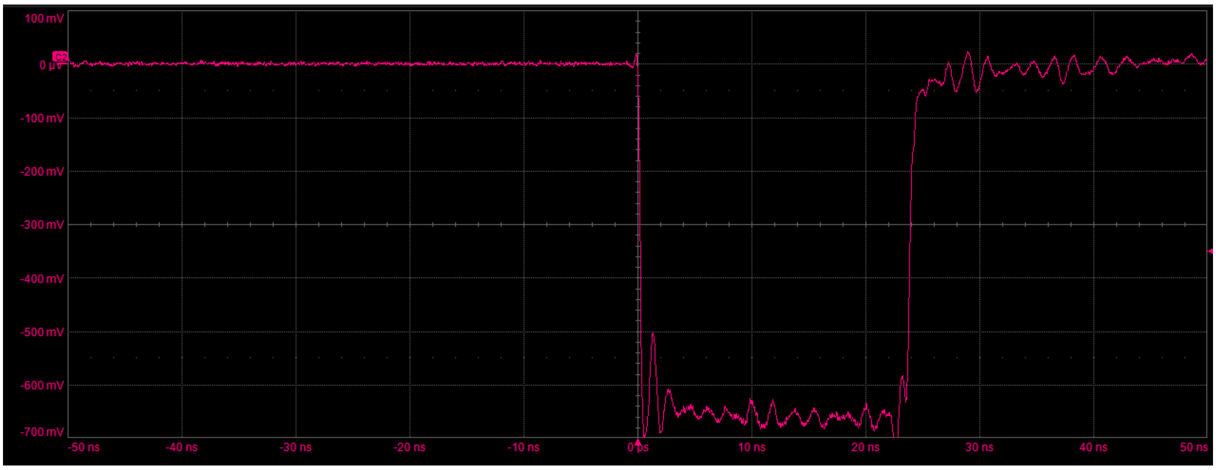

Figure 3.2: NIM pulse signal detected by oscilloscope, approximately -700 mV deep and 20 ns wide

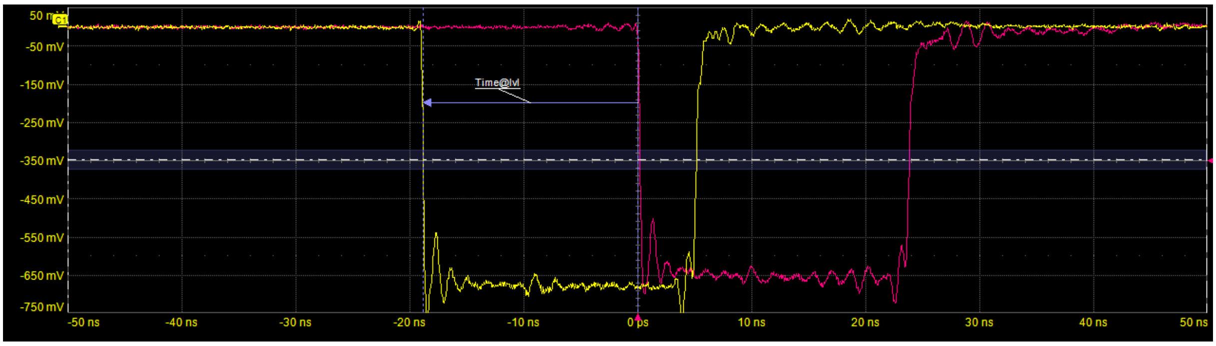

Figure 3.3: Time@level operation of digital oscilloscope which records the timing separation between the detection of consecutive pulse signals

The oscilloscope records the timing separation between the detection of two consecutive NIM pulses. The recorded timing separations are then plotted into a histogram, with 500 bins over the hold-off timing of 20 ns. This is done so each bin size is 40 ps, which matches the timing jitter of the APDs used. The measurements were also set to be performed in sequences of 1000 coincidence events to minimise processing time required to process each event individually.

3.2 Mercury Lamp

For the mercury lamp emission line at 546nm, photon coincidence events were recorded to a pre-set total of 250000 events, taking slightly over 2 hours. The histogram of the two-photon coincidence events are plotted in figure 3.4. The intensity correlation function ($g^{(2)}$) is calculated by normalising this baseline of the histogram to 1.

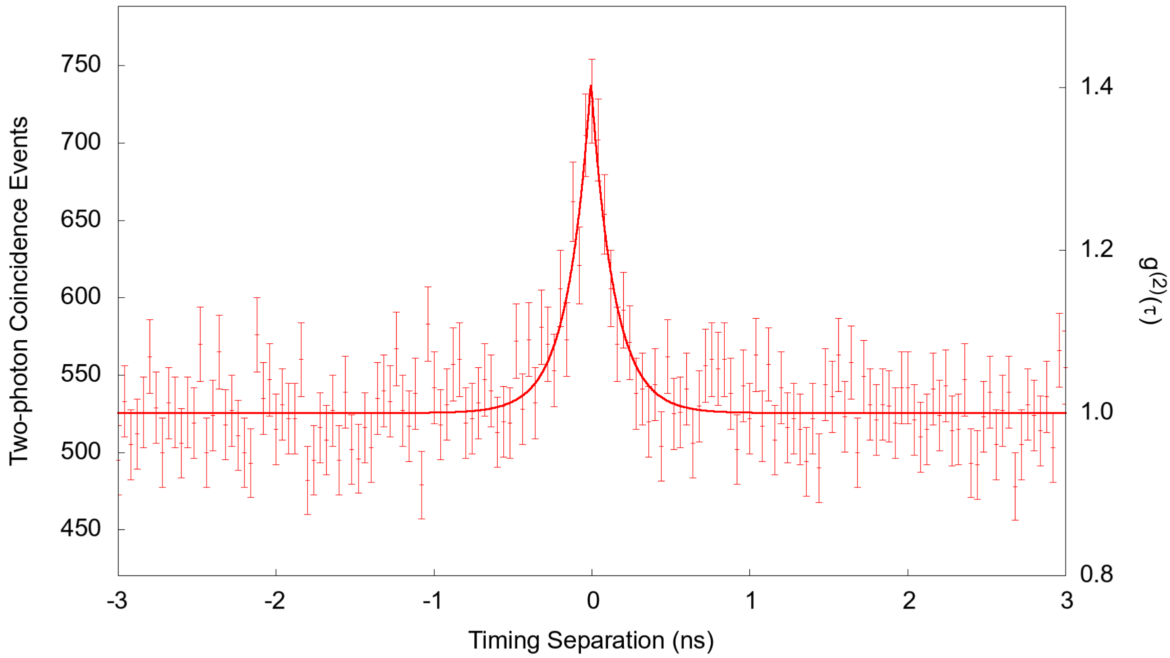

Figure 3.4: Intensity correlation ($g^{(2)}(\tau)$) of Mercury lamp. Error bars indicate uncertainties due to Poissonian counting statistics.

Here, we assume that light from the Hg lamp to have a lifetime-broadened with a Lorentzian lineshape [Fox, 2006]

$$g^{(2)}(\tau) = 1 + e^{\frac{-2|\tau|}{\tau_c}} \tag{3.2}$$

and we model it using the following equation.

$$g^{(2)}(\tau) = a + be^{\frac{-2|c-x|}{d}} \tag{3.3}$$

Using this model, the degree of photon-bunching, $g^{(2)}(\tau{=}0)$ is represented by $\frac{a}{b}$, while the coherence time τ_c is modelled by parameter d.

From the numerical fit, we obtain a $g^{(2)}(\tau{=}0)$ value of 1.41 ± 0.04 and a coherence time τ_c of 0.292 ± 0.035 ns with a reduced χ^2 value of 0.899. The difference between the measured $g^{(2)}(\tau{=}0)$ of 1.4 and the expected value of 2 is likely due to the 40 ps timing jitter of the photodetectors. Further, a study on the photodetector timing behaviour [Tan et al., 2016] suggests that the timing response FWHM of APDs might be higher than its 40ps timing jitter, which can lower the $g^{(2)}(\tau{=}0)$ value further.

3.3 Narrowband Spectral Filtering

Previous attempts to observe photon bunching from thermal light sources with short coherence time [Liu et al., 2014][Tan et al., 2014],[Deng et al., 2019] makes use of spectral filters to increase the coherence time of the light source such that it is longer than the timing resolution of the detector.

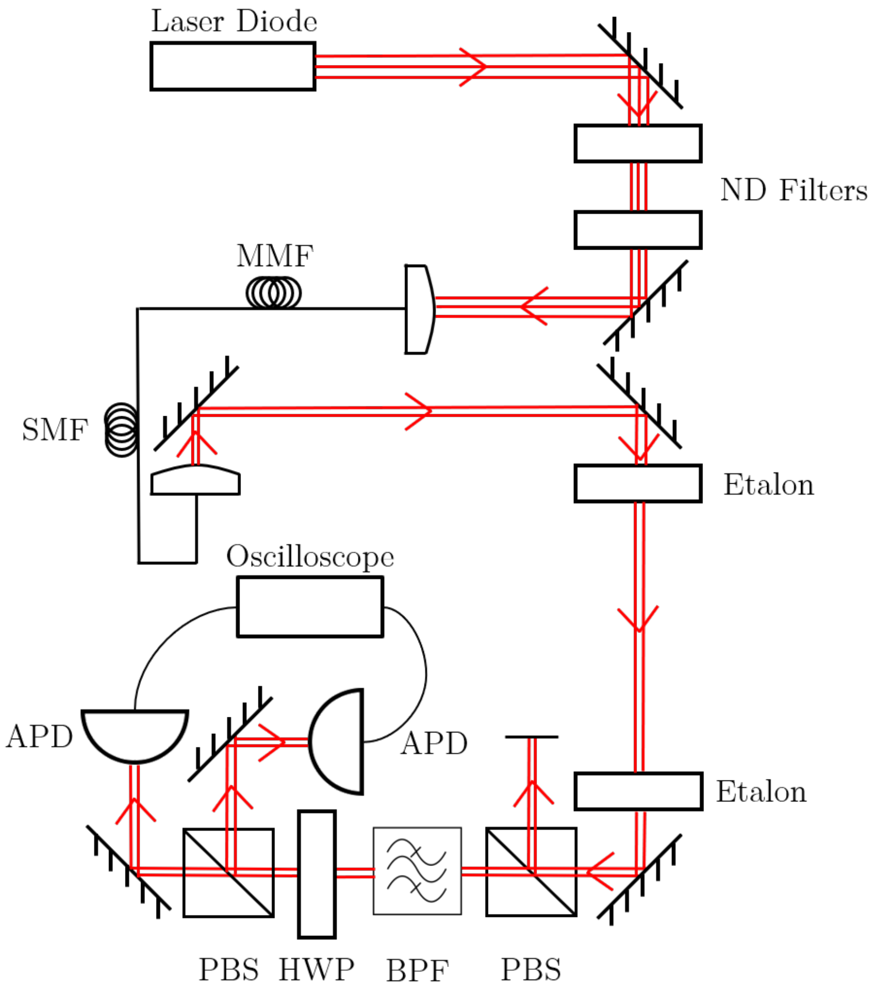

Figure 3.5: Experimental setup for a two-photon coincidence measurement, with addition of spectral filter

In this experiment, to measure the intensity correlation of the laser diode, we need a narrowband light with coherence time τ_c which is about an order of magnitude larger than the the timing jitter of the APDs used (40ps). Using

$$\begin{aligned} \Delta\nu &\approx \frac{1}{\tau_c} \\ &= \frac{1}{400\,ps} \\ &= 2.5\,GHz \end{aligned} \tag{3.4}$$

we determine the linewidth of the filtered light required to be $\leq$ 2.5 GHz.

We thus modify the experimental setup in figure 3.1, most notably to include a etalon stack to filter the light from the laser diode. The modified setup is shown in figure 3.5.

Similar to the setup in figure 3.1, we couple light from a Thorlabs L515A1 laser diode into a multimode fibre (Thorlabs M31L02) and subsequently into a single mode fibre (Thorlabs P5-460A). Light exiting from the SMF is then collimated by an aspheric lens (Thorlabs C220), with a effective focal length (EFL) of 11 mm to obtain a collimated beam of beam size 3mm. This allows us to achieve a Rayleigh length of

$$z_R = \frac{\pi \omega_0^2}{\lambda} = 54.6m \tag{3.5}$$

which is larger than the optical path of the setup (∼1m). We thus approximate that the beam stays collimated through the setup, which helps to avoid the frequency 'walk-off' effects present when the incoming beam is not normal-incident on the etalons [Green, 1980].

The beam then passes through two etalons of different thicknesses. The material of the etalons used is fused silica (Suprasil311), with a refractive index of approximately 1.46, and a 97% reflectivity coating centred at 546nm. At the centre wavelength of the laser diode, 518nm, the reflectivity is measured to be approximately 92% [Tan, 2015].

The free spectral range (FSR) of an etalon is given by [Fox, 2006]

$$\begin{aligned} FSR &= \frac{c}{2nd} \\ &= \frac{2.99 \times 10^8 \, m/s}{2 \times 1.46 \times d} \end{aligned} \tag{3.6}$$

where c is the speed of light, n is the refractive index of the material, and d is the thickness of the etalon. By stacking the two etalons, we are able to obtain an effective FSR which is the lowest common multiple of the two individual FSR values. Thus, we choose to use a 0.5mm and 0.3mm etalon from Laseroptik as it gives us a larger effective FSR, compared to an etalon thickness which is a multiple of another. The individual FSR are calculated to be 205 GHz and 341 GHz respectively, and the etalon stack has an effective FSR of 1.02 THz.

However, we note that the quoted uncertainty of etalon thickness d by Laseroptik is ±5%, which means that the individual FSR of the two etalons range from approximately 195 GHz $<$ FSR $<$ 215 GHz and 324 GHz $<$ FSR $<$ 358 GHz respectively. Thus, the effective FSR of 1.02 THz determined only serves as a guide.

Using the finesse (F) of the etalons given by [Fox, 2006],

$$\begin{aligned} F &= \frac{\pi(R_1R_2)^{\frac{1}{4}}}{1-\sqrt{R_1R_2}} \\ &= 37.7 \end{aligned} \tag{3.7}$$

where $R_1 = R_2$ is the reflectivity of the etalons, we can calculate the transmission bandwidth, $\Delta\nu$, which is given by

$$\Delta\nu = FSR \times \frac{1}{F} \tag{3.8}$$

The transmission bandwidth of the 0.5mm and 0.3mm etalons are calculated to be 5.43 GHz and 9.06 GHz. Likewise, due to the uncertainty in the thickness of the etalon, the transmission bandwidth determined here only serves as a guide. Further, we note here that the transmission bandwidth of the 0.5mm etalon is larger than the previously calculated value of 2.5GHz that we had hoped to filter. However, due to the timing constraints of the project, we decided to carry on the experiment with the current set of etalons.

To maximise the transmission of light from the laser diode through the etalon stack, we need to line the transmission bandwidth of the etalons to the frequency peak of the laser diode. We do this by tuning the temperature of the etalons, as explained in section 3.4.

Similar to section 3.1, the Calcite Glan-Taylor polariser (Thorlabs GT10) after the etalon stack selects a highly linearly polarised light in the transmission arm. The transmitted beam is rotated by a half-wave plate (HWP) to balance the count rates in the two APDs.

After the HWP, the beam then passes through a bandpass filter (BPF) centred at 546nm, with a stated FWHM of 3nm. The BPF is tilted to shift the central transmission wavelength to 518nm to match the central emission wavelength of the laser diode. The transmission wavelength after the the tilt is given by

$$\lambda(\theta) = \lambda_0\sqrt{1-\left(\frac{\sin\theta}{n}\right)^2} \tag{3.9}$$

where $\lambda(\theta)$ is the wavelength of the transmitted beam, $\lambda_0$is the wavelength of the incident beam, θ is the angle of tilt, and n is the refractive index of the BPF. Using n = 1.46, $\lambda(\theta)$ = 518 nm, λ_0 = 546 nm, we calculate θ to be 28.3°. In the setup, the bandpass filter was tilted to approximately 28°, and with further fine adjustments to maximise the count rate of the beam by varying the angle of tilt.

To measure the transmission spectrum of the bandpass filter (BPF) after the tilt, we compare the spectrum of the light beam from the laser diode with and without the bandpass filter.

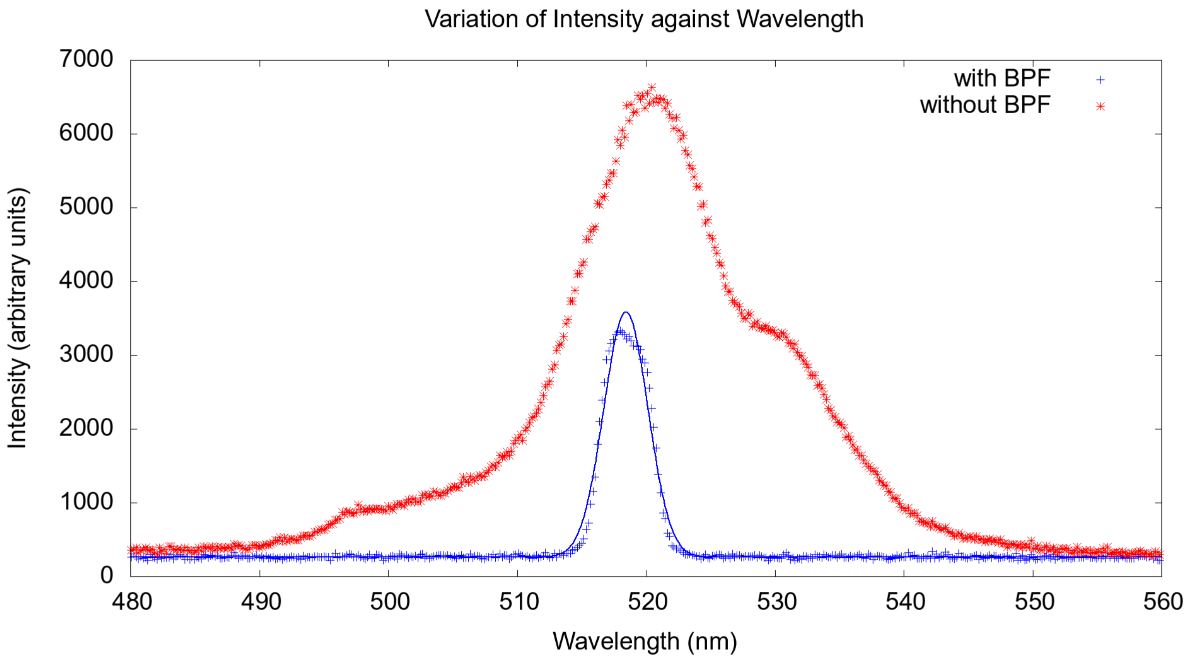

Figure 3.6: Transmission spectrum of laser diode with addition of BPF, current = 25.000 mA, temperature = 20°C

We fit the spectrum of the transmitted light through the bandpass filter using

$$Intensity = a\frac{1}{b\sqrt{2\pi}}e^{-\frac{1}{2}(\frac{x-c}{b})^2} + d \tag{3.10}$$

and obtain a spectral FWHM of 4.0 ± 0.1 nm.

The bandpass filter at ≈518 nm also helps to suppress cross-talk coincidence events from the breakdown flash of the APDs, which has an emission peak at around 850 nm [Kurtsiefer et al., 2001].

After the BPF, the beam passes through a PBS (Thorlabs PBS251). The transmitted and reflected beams are collected by aspheric lens (Thorlabs C220) into the APDs, which is connected to a digital oscilloscope for time-stamping. A photo of the setup is shown in figure 3.7.

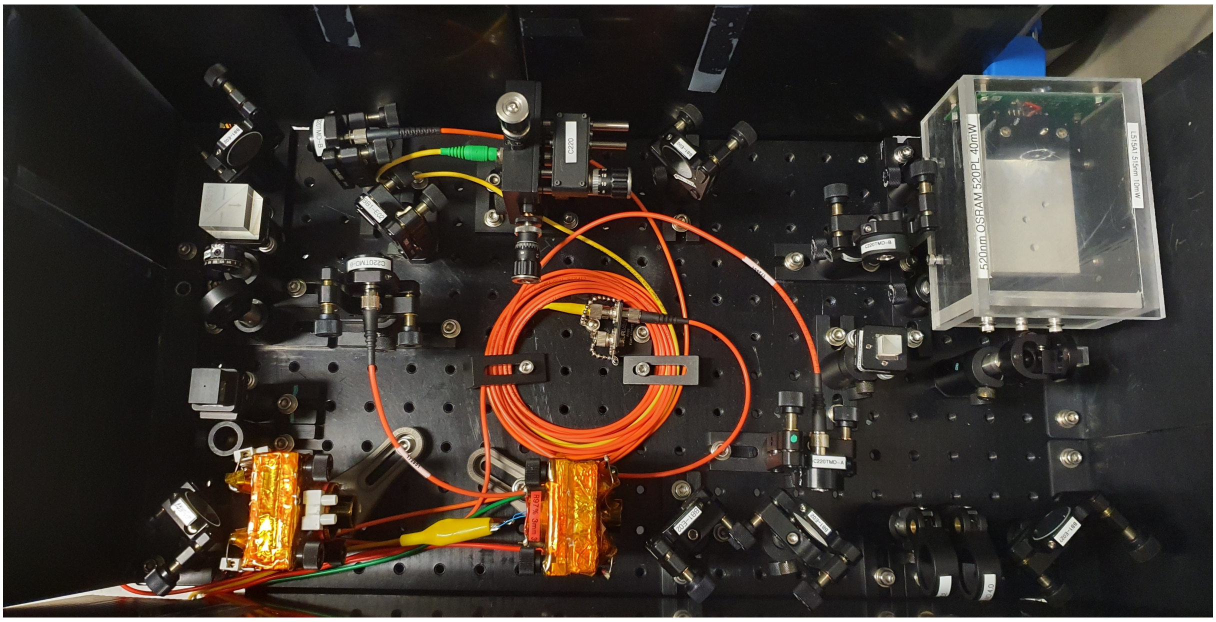

Figure 3.7: Photo of setup to determine temporal correlation of light from laser diode

3.4 Temperature Tuning of Etalon

To vary the transmission wavelength through an etalon, temperature control was chosen instead of tilting, to avoid alignment issues, losses [Leeb, 1975] and frequency 'walk-off' effects [Park et al., 2005].

The refractive index of optical materials is characterised by the empirical Sellmeier equation [Sellmeier, 1872]. For Suprasil311, the refractive index depends on wavelength via

$$n^2(\lambda) = 1 + \frac{B_1\lambda^2}{\lambda^2 - C_1} + \frac{B_2\lambda^2}{\lambda^2 - C_2} + \frac{B_3\lambda^2}{\lambda^2 - C_3} \tag{3.11}$$

Coefficients	Values
B1	7.99316057 $\times 10^{-1}$
B2	3.04794111 $\times 10^{-1}$
B3	8.85442870 $\times 10^{-1}$
C1	5.34990808 $\times 10^{-3}$
C2	1.47511317 $\times 10^{-2}$
C3	9.66383219 $\times 10^{1}$

Table 3.1: Empirical sellmeier coefficient values for Suprasil311, provided by Schott AG

To calculate the change of the refractive index of Suprasil311 when temperature is varied, we differentiate the above equation, and simplify it to obtain

$$2n\frac{dn(\lambda,T)}{dT} = (n^2-1)\left(D_0 + 2D_1\Delta T + 3D_2\Delta T^2 + \frac{E_0 + 2E_1\Delta T}{\lambda^2 - \lambda_{TK}^2}\right) \tag{3.12}$$

Coefficients	Values
D0	2.18 $\times 10^{-5}$
D1	2.45 $\times 10^{-8}$
D2	-2.72 $\times 10^{-11}$
E0	2.31 $\times 10^{-7}$
E1	2.21 $\times 10^{-10}$
λ_{TK}	235 nm

Table 3.2: Derivative coefficient values for Suprasil311, provided by Schott AG

With reference to the empirically determined Sellmeier coefficients provided by Schott AG, we obtain a tuning rate of -4.1 GHz/K. This allows us to cover the 205GHz FSR of a 0.5 mm etalon by tuning the temperature from a room temperature of 25°C to 75°C.

We attempt to maximise the transmission of laser light from the laser diode through the etalons. To achieve this, we first set the input current of the laser diode to 40 mA, where we can reasonably assume that the laser diode is in the lasing regime. Next, we control the temperature of the etalons through a proportional-integral-derivative (PID) controller by heating a set of 4 resistors, and using a thermistor to provide temperature readings. As the etalons are heated, when the linewidth of the laser light falls within the transmission bandwidth of the etalons, we expect to see an increase in the photon count rate on the APDs.

We start by heating the 0.5 mm etalon from 25°C to 75°C, and monitor the count rates detected by the APDs. We note the temperature at which the count rates reaches a maximum. We then turn off the heating element and cool the etalon back down to 25°C, and once again note down the temperature at which the count rate is at a maximum. Using these two temperature readings as reference, we vary the temperature of the etalon to maximise the photon count rate. Once the 0.5 mm etalon has been tuned, we repeat a similar procedure for the 0.3 mm etalon.

3.5 Results

We measure the two-photon coincidence events of the laser diode with an input current of 30.00 mA, at a count rate of about 1×10^6 counts/s for 300 s, and plot a histogram of the events in figure 3.8.

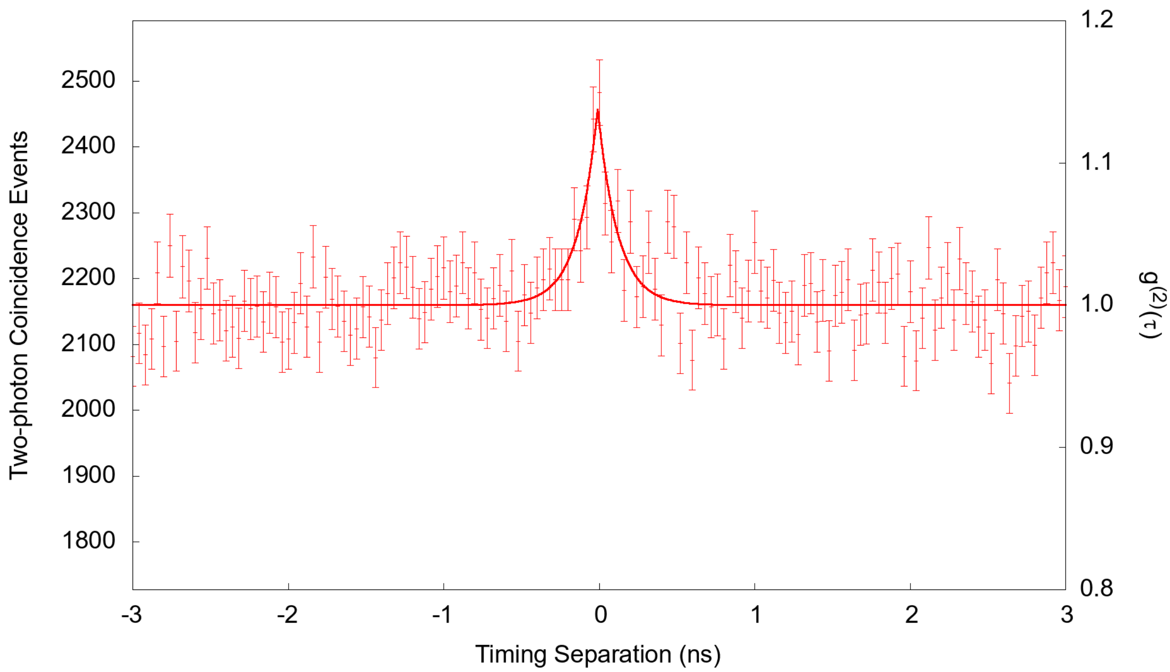

Figure 3.8: Intensity correlation ($g^{(2)}(\tau)$) of laser diode, current = 30.00mA, 40 ps time bins. Error bars indicate uncertainties due to Poissonian counting statistics.

We model the two-photon coincidence events to a Lorentzian line shape which approximates the transmission function through the etalons. The equation of fit used here is

$$g^{(2)}(\tau) = a + be^{\frac{-2|c-x|}{d}} \tag{3.13}$$

The peak photon correlation, $g^{(2)}(\tau{=}0)$ is normalised by the parameters $\frac{a}{b}$, while the coherence time τ_c is modelled by parameter d.

From the fitted parameters, we obtain a $g^{(2)}(\tau{=}0)$ value of 1.14 ± 0.02 and a coherence time τ_c of 0.256 ± 0.048 ns with a reduced χ^2 value of 0.958. The value of τ_c here likely reflects the actual transmission bandwidth of the laser diode through the etalon stack,

$$\begin{aligned} \Delta\nu &\approx \frac{1}{\tau_c} \\ &= \frac{1}{256\,ps} \\ &= 3.91\,GHz \end{aligned} \tag{3.14}$$

The $g^{(2)}(\tau{=}0)$ value of 1.14 suggests that the light emitted by this laser diode at 30.00 mA is indeed bunched light. However, this differs from the expected value of 2 (refer to section 1.4). Apart from the aforementioned timing uncertainty of the photodetectors, there could be several possible reasons for this.

The effective free spectral range (FSR) of the etalon stack was previously calculated to be 1.02 THz (neglecting the uncertainty of the etalon thickness). With a bandpass filter transmission bandwidth of 4.0 nm (refer to figure 3.6), 3 to 4 transmission peaks of the etalon stack fall into the transmission band of the bandpass. Since the coherence time of the light from different transmission peaks has a coherence time shorter than the APDs (in the order of 10^{-12}s), this reduces the photon bunching signal in the resolution timescale of the detectors (in the order of 10^{-11}s). Further, the reflectivity of the etalons reduces from 97% at the design wavelength of 546 nm to 92% at 518 nm. Since frequencies that are out of resonance of the etalons are suppresed by a factor of 1-R [Fox, 2006], the suppression of the etalons is lower at 518nm, which leads to more noise contribution from the suppressed wavelengths. The lower signal-to-noise ratio reduces the value of $g^{(2)}(\tau{=}0)$.

We then vary the laser diode input current from 30.00 mA to 36.00 mA in step size of 0.01 mA. We perform the same two-photon coincidence measurement for an integration time of 300 s at each input current value.

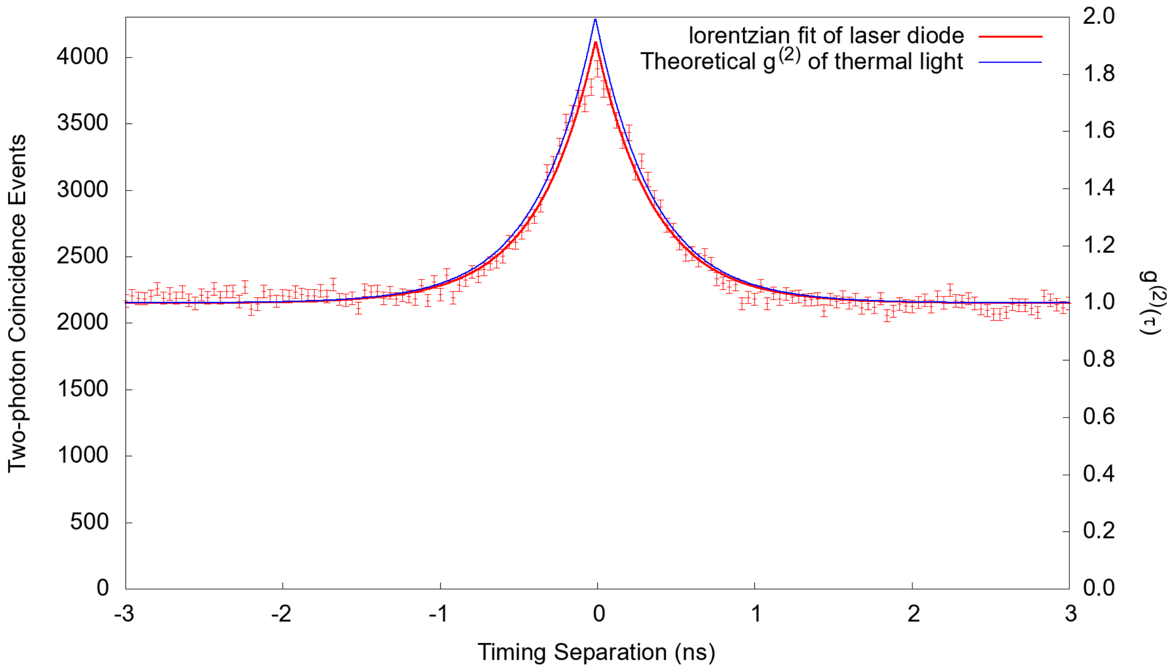

Figure 3.9: Intensity correlation ($g^{(2)}(\tau)$) of laser diode, current = 31.51 mA, 40 ps time bins. Error bars indicate uncertainties due to Poissonian counting statistics.

Figure 3.9 shows the histogram of photon coincidence events as the input current value is increased to 31.51 mA. We observe an increase in the extent of photon bunching, as the fitted $g^{(2)}(\tau{=}0)$ has a value of 1.92 ± 0.02 ($\chi^2 = 1.77$). Moreover, we see that the coherence time also increases to $\tau_c = 0.722 \pm 0.019$ ns.

This suggests that as input current increases, the linewidth of the light from the laser diode starts to narrow, as evidenced by the increase in τ_c. We calculate the linewidth $\Delta\nu$ to be

$$\begin{aligned}\Delta\nu &\approx \frac{1}{\tau_c} \\ &= \frac{1}{722\,ps} \\ &= 1.39\,GHz\end{aligned} \tag{3.15}$$

However, from the high $g^{(2)}(\tau{=}0)$ value, we deduce that the light from the laser diode still behaves as a thermal light. This signals that as the input current to a laser diode increases, the linewidth of the light starts to decrease before the photon statistics of the light changes from thermal to coherent.

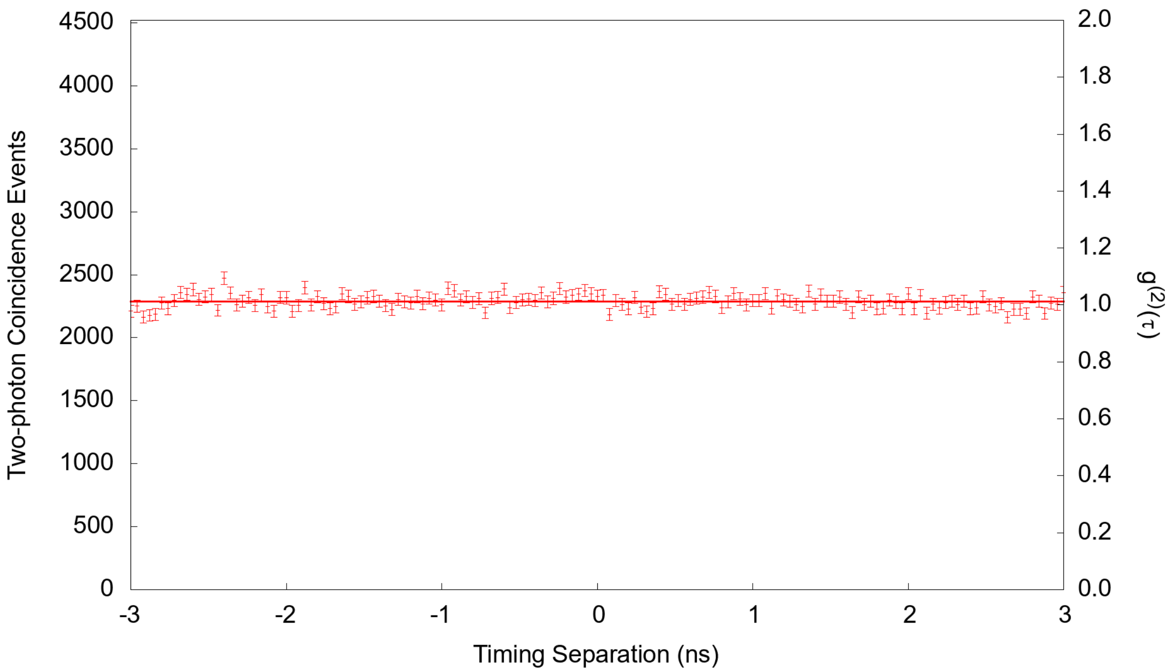

Figure 3.10: Intensity correlation ($g^{(2)}(\tau)$) of laser diode, current = 36.00 mA, 40 ps time bins. Error bars indicate uncertainties due to Poissonian counting statistics.

As the input current increases further to 36.00 mA, the $g^{(2)}$ function flattens out, and the laser diode is better modelled by a coherent light source.

3.6 Evolution of Coherence

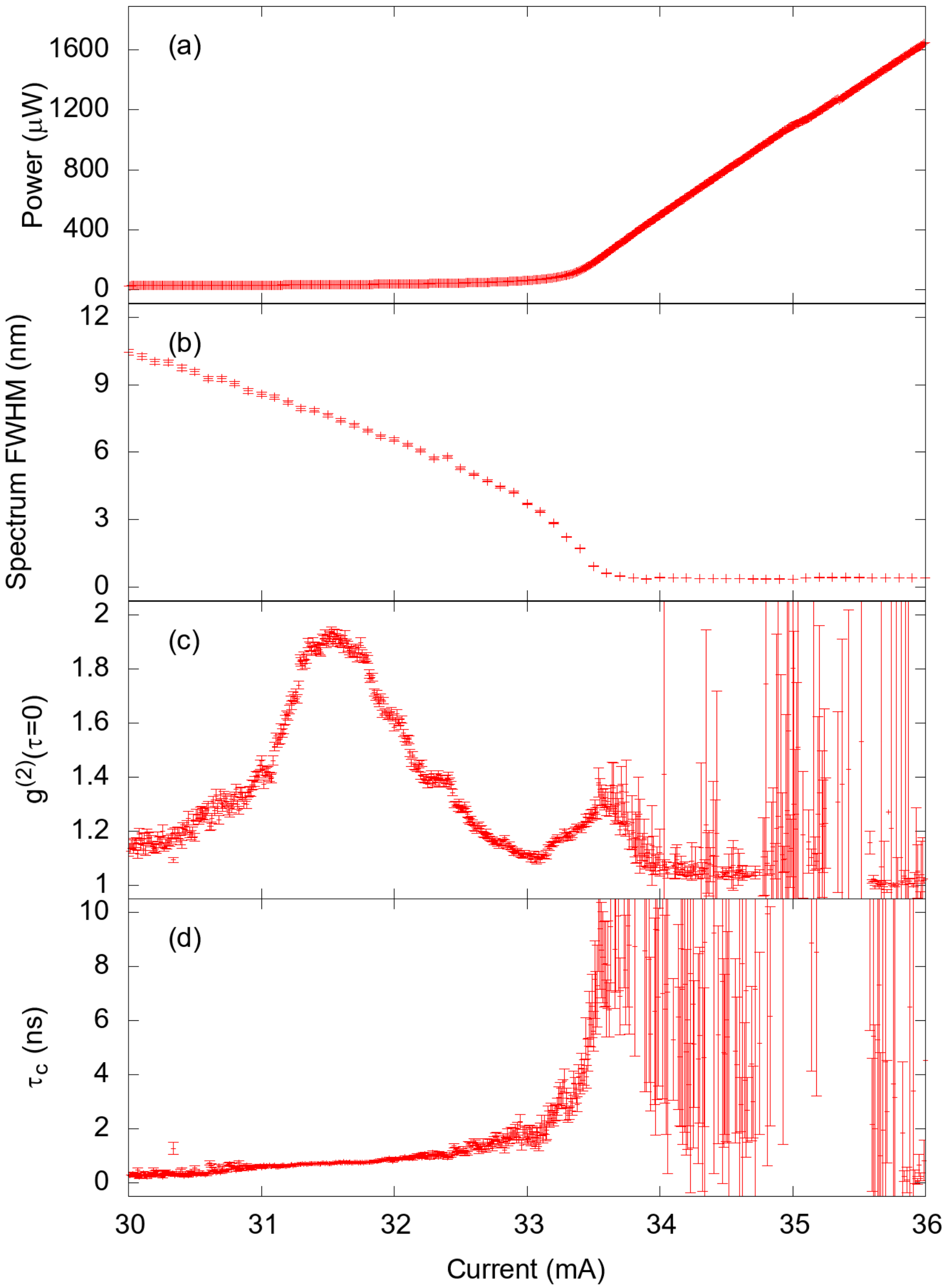

Figure 3.11: Evolution of power, linewidth, $g^{(2)}(\tau=0)$, and τ_c of a laser diode with input current

From figure 3.11, as the input current increases from 30.00 mA to around 31.51 mA, $g^{(2)}(\tau{=}0)$ increases from 1.14 to 1.92. This corresponds to an increase in the τ_c, which suggests that the linewidth of the beam sampled is no longer limited by the transmission spectrum of the etalons. According to equation 3.2, this allows us to resolve the $g^{(2)}(\tau{=}0)$ closer to the theoretical expectation of 2.

As the input current increases beyond 31.51 mA, while we see that the τ_c still increase, the value of $g^{(2)}(\tau{=}0)$ starts to decrease as well. This indicates that the photon-bunching signal decreases, which suggests the start of a transition from thermal to coherent light.

The decrease in $g^{(2)}(\tau{=}0)$ continues until approximately 34.00 mA. As the input current increases beyond 34.00 mA, the Lorentzian model fits the data worse, as shown by the significantly larger error bars from the fit.

We also fit the two-photon coincidence events to a linear model with a gradient of 0 (i.e. a constant value), and normalise the photon correlation to 1, which reflects the theoretical prediction of the coherence of laser light

$$g^{(2)}(\tau) = 1 \tag{3.16}$$

We compare the reduced χ^2 value of the Lorentzian and linear fit, and plot it against the change in input current in figure 3.12.

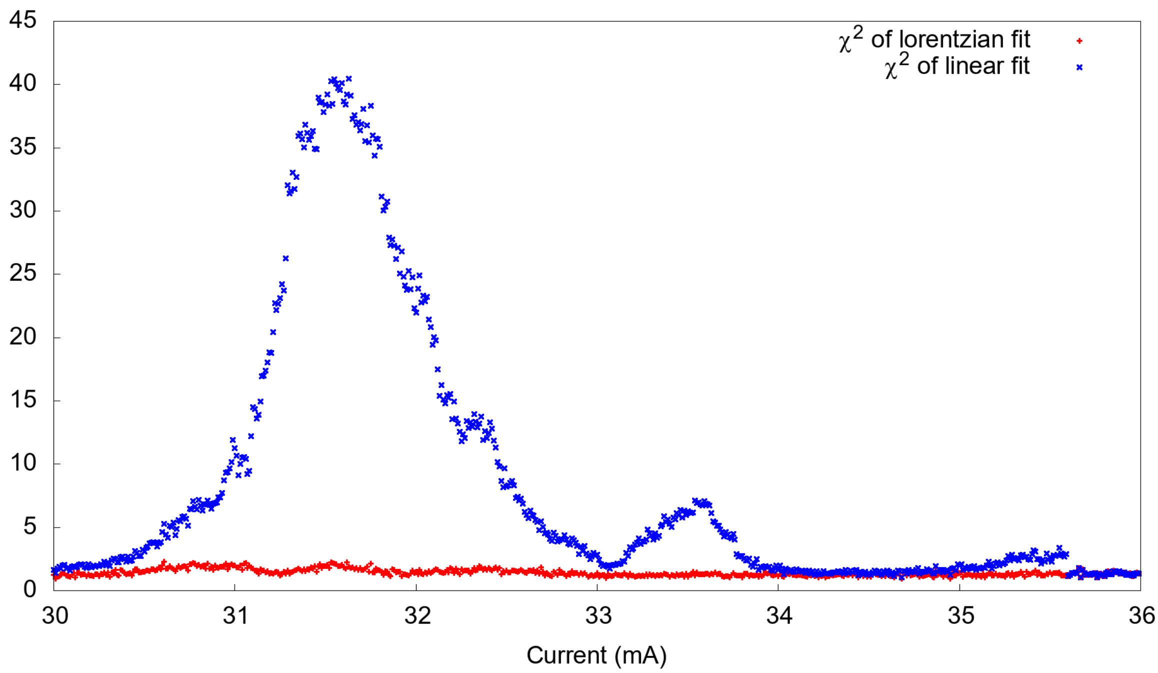

Figure 3.12: χ^2 values of lorentzian and linear fit

From figure 3.12, we see that the linear model has a χ^2 value which starts to approach unity as the input current (I) increases beyond 34.00 mA. We thus replot the $g^{(2)}(\tau{=}0)$ values against input current in figure 3.13 using the Lorentzian model for $I < 34.00$ mA, and the linear model for $I \geq 34.00$ mA.

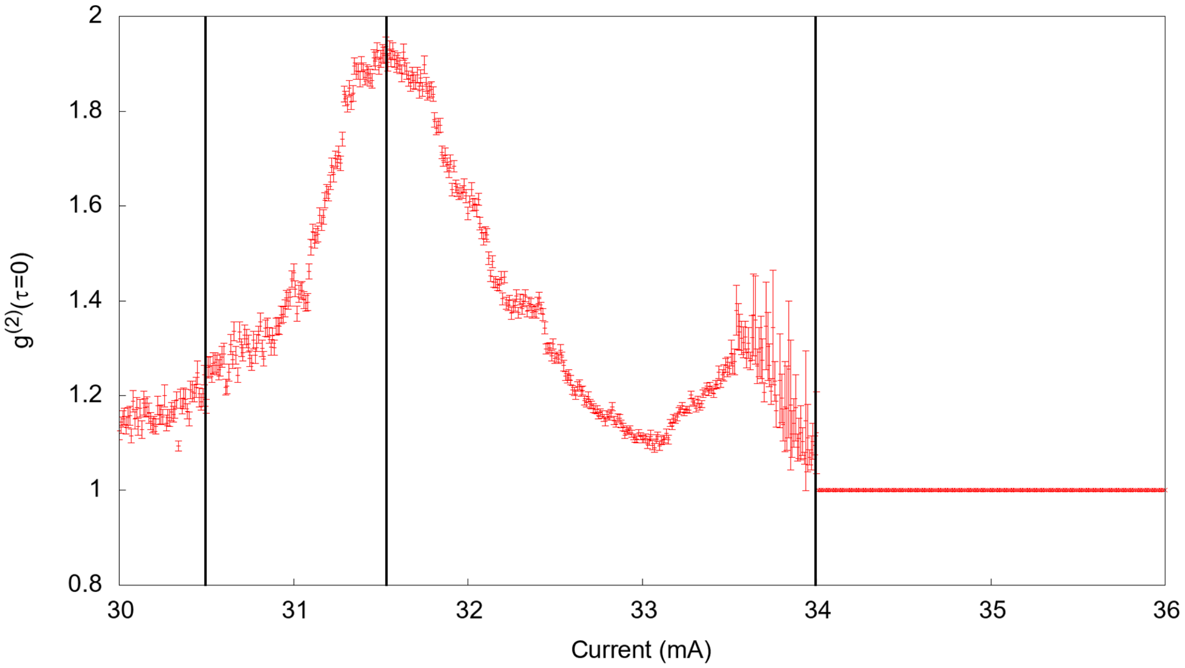

Figure 3.13: $g^{(2)}(\tau{=}0)$ values by combining Lorentzian model for $I < 34.00$ mA and linear model for $I \geq 34.00$ mA

From figure 3.13, we can separate the graph into four general regimes. In the first regime, where $I < 30.50$ mA, the transmission linewidth of the laser diode is limited by the etalon stack, which indicates that the light emitted by the laser diode has a broad band which still acts as an LED. In region 2, $30.50\,\text{mA} < I < 31.51$ mA, the linewidth of the laser diode decreases, but the light emitted still bunches, signalling the first phase of a transition from LED to laser. In region 3, $31.51\,\text{mA} < I < 34.00$ mA, the linewidth of the laser diode continues to decrease and the photon stream becomes increasingly random, which indicates a second phase of transition. Finally, in region 4, where $I > 34.00$ mA, the laser diode can be described as a coherent light source.

Chapter 4

Summary & Outlook

Although the first laser was demonstrated 60 years ago, the evolution of a laser diode's temporal coherence with input current has yet to be experimentally verified. Since evidence for coherence (measured in terms of the second order correlation function $g^{(2)}$) is generally regarded as a trait of traditional laser action [Blood, 2013], it is important for us to quantify the onset of coherence in a laser diode.

In this report, we first identified the approximate LED, transition, and lasing regime of a laser diode via the P-I curve. Generally, a laser diode is thought to make the transition from LED to lasing at the kink in the P-I curve, or the 'lasing threshold'. We then verify this transition regime by measuring the spectral FWHM of the light emitted by the laser diode. Determining the transition regime to be around $32\,\mathrm{mA} < \mathrm{I} < 34\,\mathrm{mA}$, we conduct further experiments to quantify the temporal coherence of the laser diode in this neighbourhood, from 30 mA to 36 mA.

As a proof of concept, we first measure the second-order correlation of a quasi-thermal source, mercury lamp, and obtain a $g^{(2)}(\tau{=}0)$ value of 1.41 ± 0.04 and a coherence time τ_c of 0.292 ± 0.035 ns. This shows that our setup is generally capable of resolving $g^{(2)}(\tau{=}0)$ to be significantly more than 1 for a incoherent source.

We then change the light source to a laser diode and add a narrowband spectral filter by stacking two etalons to obtain a transmission band measured to be about 3.91 GHz. This allows us to photon bunching signal of $g^{(2)}(\tau{=}0) = 1.14 \pm 0.02$ at input current value of 30.00 mA, with a etalon-limited coherence time of 0.256 ± 0.048 ns.

As the input current increases, the photon bunching signal increases to $g^{(2)}(\tau{=}0) = 1.92 \pm 0.02$ while the coherence time increases to $\tau_c = 0.722 \pm 0.019$ ns at 31.51 mA. As the input current increases further, τ_c continues increasing, but the value of $g^{(2)}(\tau{=}0)$ begins to drop. This suggests that the light beam from the laser diode undergoes a transition from LED to laser, by first decreasing its linewidth, and subsequently emitting light in a more statistically random manner. At about 34.00 mA, the laser diode can be approximated to a coherent laser.

As a possible future step, we can verify the change in increase in coherence time of a laser diode with input current by measuring the linewidth of a laser diode using a cavity. A cavity length of about 10 cm would allow us to resolve spectral features that are about 10MHz.

We can also amend the setup to include a stack of bandpass filters with a smaller effective transmission bandwidth, up to a 1 nm transmission FWHM to only allow one transmission peak from the etalons to pass through. This could allow us to obtain a higher $g^{(2)}(\tau{=}0)$ value for the laser diode in LED, and thus better determine the input current value at which each transition phase happens.

Appendix A

Optimisation of Photon-Coincidence Events

Let the number of photo-events detected by each APD be E_1 and E_2, and

$$E_1 + E_2 = I \tag{A.1}$$

where I is the intensity of the beam exiting the Half-Wave Plate (HWP). Thus,

$$\begin{aligned} E_1 &= I - E_2, \quad \textit{or}, \\ E_2 &= I - E_1 \end{aligned} \tag{A.2}$$

Since a two-photon coincidence is only observed when two separate photo-events are detected by the two detectors, the coincidence rate,

$$\begin{aligned} C &\propto E_1 \times E_2 \\ &\propto E_1 \times (I - E_1) \end{aligned} \tag{A.3}$$

For maximum coincidences events,

$$\begin{aligned} \frac{d}{dE_1}(E_1 \times (I - E_1)) &= 0 \\ \implies I - 2E_1 &= 0 \\ \implies E_1 &= \frac{I}{2} = E_2 \end{aligned} \tag{A.4}$$

Bibliography

[Blood, 2013] Blood, P. (2013). The laser diode: 50 years on. *IEEE Journal of Selected Topics in Quantum Electronics*, 19(4):1503201–1503201.

[Chow et al., 2014] Chow, W. W., Jahnke, F., and Gies, C. (2014). Emission properties of nanolasers during the transition to lasing. *Light: Science & Applications*, 3(8):e201–e201.

[Deng et al., 2019] Deng, Y.-H., Wang, H., Ding, X., Duan, Z.-C., Qin, J., Chen, M.-C., He, Y., He, Y.-M., Li, J.-P., Li, Y.-H., et al. (2019). Quantum interference between light sources separated by 150 million kilometers. *Physical review letters*, 123(8):080401.

[Einstein, 1917] Einstein, A. (1917). Zur quantentheorie der strahlung. *Phys. Z.*, 18:121–128.

[Fox, 2006] Fox, M. (2006). *Quantum optics: an introduction*, volume 15. OUP Oxford.

[Glauber, 1963] Glauber, R. J. (1963). The quantum theory of optical coherence. *Physical Review*, 130(6):2529.

[Gordon et al., 1955] Gordon, J. P., Zeiger, H. J., and Townes, C. H. (1955). The maser—new type of microwave amplifier, frequency standard, and spectrometer. *Physical Review*, 99(4):1264.

[Green, 1980] Green, J. (1980). The'walk-off'effect in fabry-perot etalons-limitations to'single-shot'linewidth measurements at longer wavelengths. *Journal of Physics E: Scientific Instruments*, 13(12):1302.

[Hanbury Brown and Twiss, 1956] Hanbury Brown, R. and Twiss, R. Q. (1956). A test of a new type of stellar interferometer on sirius. *Nature*, 178(4541):1046–1048.

[Kurtsiefer et al., 2001] Kurtsiefer, C., Zarda, P., Mayer, S., and Weinfurter, H. (2001). The breakdown flash of silicon avalanche photodiodes-back door for eavesdropper attacks? *Journal of Modern Optics*, 48(13):2039–2047.

[Leeb, 1975] Leeb, W. R. (1975). Losses introduced by tilting intracavity etalons. *Applied physics*, 6(2):267–272.

[Liu et al., 2014] Liu, X.-F., Chen, X.-H., Yao, X.-R., Yu, W.-K., Zhai, G.-J., and Wu, L.-A. (2014). Lensless ghost imaging with sunlight. *Optics letters*, 39(8):2314–2317.

[Maiman, 1960] Maiman, T. H. (1960). Stimulated optical radiation in ruby. *Nature*, 187(4736):493–494.

[Mandel and Wolf, 1995] Mandel, L. and Wolf, E. (1995). *Optical coherence and quantum optics*. Cambridge university press.

[Ning, 2013] Ning, C.-Z. (2013). What is laser threshold? *IEEE Journal of Selected Topics in Quantum Electronics*, 19(4):1503604–1503604.

[Park et al., 2005] Park, S., Ko, H., and Park, M.-H. (2005). Distortion of gaussian intensity profile by passing through a tilted fabry-perot filter. *Optical Engineering*, 44(4):048001.

[Saleh and Teich, 2019] Saleh, B. E. and Teich, M. C. (2019). *Fundamentals of photonics*. John Wiley & Sons.

[Schawlow and Townes, 1958] Schawlow, A. L. and Townes, C. H. (1958). Infrared and optical masers. *Physical Review*, 112(6):1940.

[Sellmeier, 1872] Sellmeier, W. (1872). Iii. ueber die durch die aetherschwingungen erregten mitschwingungen der körpertheilchen und deren rückwirkung auf die erstern, besonders zur erklärung der dispersion und ihrer anomalien. *Annalen der Physik*, 221(3):399–421.

[Tan, 2015] Tan, P. K. (2015). *Stellar Temporal Intensity Interferometry*. PhD thesis.

[Tan et al., 2016] Tan, P. K., Chan, A. H., and Kurtsiefer, C. (2016). Optical intensity interferometry through atmospheric turbulence. *Monthly Notices of the Royal Astronomical Society*, 457(4):4291–4295.

[Tan et al., 2014] Tan, P. K., Yeo, G. H., Poh, H. S., Chan, A. H., and Kurtsiefer, C. (2014). Measuring temporal photon bunching in blackbody radiation. *The Astrophysical Journal Letters*, 789(1):L10.

[Ulrich et al., 2007] Ulrich, S., Gies, C., Ates, S., Wiersig, J., Reitzenstein, S., Hofmann, C., Löffler, A., Forchel, A., Jahnke, F., and Michler, P. (2007). Photon statistics of semiconductor microcavity lasers. *Physical review letters*, 98(4):043906.

[Wang et al., 2017] Wang, T., Aktas, D., Alibart, O., Picholle, É., Puccioni, G. P., Tanzilli, S., and Lippi, G. L. (2017). Nontrivial photon statistics in small scale lasers. *arXiv preprint arXiv:1710.02052*.

[Wiersig et al., 2009] Wiersig, J., Gies, C., Jahnke, F., Aßmann, M., Berstermann, T., Bayer, M., Kistner, C., Reitzenstein, S., Schneider, C., Höfling, S., et al. (2009). Direct observation of correlations between individual photon emission events of a microcavity laser. *Nature*, 460(7252):245–249.

[Zou and Mandel, 1990] Zou, X. and Mandel, L. (1990). Photon-antibunching and sub-poissonian photon statistics. *Physical Review A*, 41(1):475.